buildings

MDPI

Article

The Detailed Axial Compression Behavior of CFST Columns Infilled by Lightweight Concrete

Bara'a R. Alnemrawi * and Rajai Al-Rousan

Department of Civil Engineering, Faculty of Engineering, Jordan University of Science and Technology, P.O. Box 3030, Irbid 22110, Jordan

* Correspondence: bralnemrawi19@eng.just.edu.jo

Abstract: The utilization of lightweight aggregate concrete (LWC) plays a major role in reducing the self-weight of CFST (concrete-filled steel tube) columns, which is reflected in the behavior of the structural system. This paper aims to investigate the characteristics of lightweight concrete-filled steel tubular (LWCFST) columns under an axial compressive load, using a total of (48) LWCFST column models. The simulated models were divided into four groups with different concrete compressive strength, length-to-diameter ratios (L/D), and diameter-to-thickness ratios (D/t). Four concrete compressive values were examined (30, 40, 50, and 60) MPa, three length-to-diameter ratios short (L/D = 3), medium (L/D = 6), and long (L/D = 9), and four diameter-to-thickness ratios (36, 31, 26, and 21). The method of nonlinear finite element analysis (NLFEA) was used to fulfill the objective of this study where results were presented as graphical plots between the compressive loading versus the axial and lateral strains along with the failure modes. In addition, the results were compared with the AISC360-16 and EC4 codes predictions to examine their applicability on the LWCFST columns where the AISC was overpredicted in most cases with higher percentages under lower (L/D) values, whereas the EC2 was underestimated in most cases with high percentages up to 28%, which become closer to the NLFEA predictions at higher (L/D) values. It has been revealed that the utilization of steel tubes significantly improves the LWCFST column's mechanical performance, ductility, compressive strength, and toughness. Moreover, the structural behavior of the LWCFST columns and their associated failure modes was found to be highly affected by the geometrical properties of the CFST column (i.e., L/D ratio and D/t ratio) where specimens with small tube thickness show bad behavior. Finally, the utilization of high-strength concrete has a favorable performance compared to the utilization of thick steel tubes.

Keywords: LWCFST columns; NLFEA; concrete strength; diameter-to-thickness; length-to-diameter

check for updates

Citation: Alnemrawi, B.R.; Al-Rousan, R. The Detailed Axial Compression Behavior of CFST Columns Infilled by Lightweight Concrete. *Buildings* **2024**, *14*, 2844. https://doi.org/10.3390/buildings14092844

Academic Editor: Duc-Kien Thai

Received: 25 July 2024
Revised: 28 August 2024
Accepted: 5 September 2024
Published: 10 September 2024

Copyright: © 2024 by the authors. Licensee MDPI, Basel, Switzerland. This article is an open access article distributed under the terms and conditions of the Creative Commons Attribution (CC BY) license (https://creativecommons.org/licenses/by/4.0/).

1. Introduction

The utilization of concrete-filled steel tubular columns (CFST) is widely recognized, due to the preferable mechanical performance of the columns and their use in several applications, including offshore buildings, tall structures, and bridges [1–7]. However, this extensive utilization is directly related to their high stiffness, strength, ductility, seismic resistance, and energy absorption capacity [8], which are directly related to the composite action developed between the steel tube and the concrete core where the applied loading during the construction stage is sustained by the steel tube during the concrete pouring. In the same context, the concrete core increases the steel tube's localized buckling and avoids the steel tube's inward buckling; these actions decrease the time and cost of construction [9–11].

Lightweight concrete (LWC) is made using lightweight aggregate obtained either from natural (scoria, tuff, and pumice) or artificial (clay, slate, fly ash, and blast-furnace slags) sources [12]. It has major advantages compared to the conventionally used normal weight concrete (NWC), with 20 to 33% less weight, higher strength-to-weight ratios (S/W), a lower

heat conductivity of 12 to 33%, improved fire resistance, sound insulation, and seismic resistance [13–15]. Despite its advantages, lightweight concrete has several disadvantages which are summarized as the higher creep and shrinkage deformations with less rigid behavior compared to NWC. The utilization of LWC improves the insulation and the thermal properties of the building structure. The artificial LWC is produced using the expanded clay aggregate (ECA) formed at high temperature (1200 °C) in a rotary kiln. The ECA has a unique spherical shape with a barely closed outer surface compared to the porous black inner surface. However, the strength of the NSC is higher compared to the LWC due to its stronger interfacial transition zone (ITZ), which is highly dependent on the aggregate properties, its source, and shape. The LWA represents the weakest component in the LWC, which limits their elastic and strength characteristics [16].

Generally, CFST columns are formed in different shapes (such as square, rectangular, and circular); however, research carried out in the literature has pointed out that the circular cross-section columns have the best performance [17,18], where stresses are uniformly distributed and the effective confinement is ensured within the concrete core. The distribution within the circular-shaped section is better than those in the rectangular or square sections, even though they are favorable in some cases for architectural purposes, especially at the beam–column connection locations where the composite action takes place between the different structural members [19–21]. Moreover, CFST columns are preferable compared to conventional reinforced concrete (RC) columns due to their smaller cross-sections required to sustain the same loading amount. In addition, pouring lightweight concrete inside the CFST tubes further reduces the weight of the CFST column, in addition to providing better seismic performance [22–24].

The behavior of the LWCFST columns has not been adequately studied in the literature as much as the behavior of the NWCCFST ones [25]. A comparative study on the behavior of LWCFST and NWCFST columns was conducted by Ghannam et al. [26] on long columns of three different columns' shapes (square, circular, and rectangle). The results revealed that the failure mode in the LWCFST and NWCFST columns was similar where columns fail in global buckling with more ductile behavior observed in the lightweight columns. In addition, the behavior of short rectangular CFST columns was studied by Mouli and Khelafi [27] using normal weight and lightweight concrete, where the LWCFST columns had higher strength compared to the NWCFST columns. The axial compression behavior of the LWCFST columns was experimentally tested by Fu et al. [28], where it was concluded that columns with high confinement ratios failed in shear mode compared to local buckling failure for columns with small confinement ratios where the different confinement ratios were obtained using different concrete compressive strengths for the concrete core. The experimentally obtained results were compared with code theoretical predictions and it was found that the Eurocode (EC) [29] has the closer predictions. Moreover, the behavior of the LWCFST columns was tested by Ji et al. [30] with different levels of slenderness, using columns of different lengths to highlight its effect on the structural behavior of the columns. It has been revealed that the slender columns' performance of more than 80 mm/mm slenderness is highly affected by the elastic instability of the structural system. Al-Eliwi et al. [31] conducted an investigatory and comparative study on the behavior of LWCFST and self-compacted concrete-filled steel tube (SCCFST) columns under the same circumstances using different (L/D) and (D/t) ratios. The study's findings indicated that the LWCFST columns performed differently from SCCFST columns, particularly in terms of ductility and failure mode. The local buckling mode predominated in LWCFST columns due to the utilization of the lightweight aggregate; this behavior was observed in LWCFST specimens with higher (L/D) ratios. On the other hand, the failure mode of long SCCFST specimens was dominated by global buckling.

Studying the behavior of axially loaded LWCFST requires the utilization of special setups, equipment, and testing machines; this therefore requires time and high costs, which is not financially feasible. Consequently, finding a suitable, feasible, and accurate method for examining the behavior of structural elements is favorable, such as the nonlinear finite

element analysis (NLFEA) method [32]. In contrast, it is challenging to find accurate and suitable experimental work that is required to validate the NLFEA models to expand the validated models for studying the behavior of other parameters [33,34]. However, the method of NLFEA has been extensively utilized in the literature and proves its efficiency in studying the behavior of different structural members, such as the CFST columns. Therefore, the experimental work conducted by Al-Eliwi et al. [19] on the behavior of LWCFST columns was used to validate the NLFEA-simulated models to ensure their accuracy and ability to be extended for the examination of the effect of other parameters. This study examines the full structural behavior of the widely utilized CFST columns poured with a lightweight concrete inner core, where the self-weight of the structural system was efficiently reduced and many advantages were found. Moreover, the LWCFST columns made of circular cross-sections had a better stress distribution, along with the developed composite action between the steel tube and the inner concrete core. In addition, it is essential to cover all the design aspects where different circumstances might be combined, such as the columns' length, steel tube thickness, and concrete compressive strength. Therefore, this study examines the effect of concrete compressive strength, length-to-diameter ratios (L/D), and diameter-to-thickness ratios (D/t) on the performance of LWCFST columns. Four concrete compressive values were examined (30, 40, 50, and 60 MPa); three length-to-diameter ratios of short (L/D = 3), medium (L/D = 6), and long (L/D = 9) and four diameter-to-thickness ratios (36, 31, 26, and 21) were also included in this study. Finally, the prediction accuracy of the simulated and code predictions was examined, where the EC4 [29] and the AISC360-16 [35] code predictions regarding the axial compressive strength of the LWCFST columns were theoretically calculated and compared with the simulated ones to provide a full view on the behavior of LWCFST columns and to highlight the different codes predictions' accuracy.

2. Research Significance

The behavior of the CFST columns was extensively investigated in the literature, where the conventional concrete was used as an infill core. However, in light of the increased weight of structural buildings, there is a tendency to reduce the structural member's self-weight, along with maintaining their performance so as to not significantly affect them. Therefore, the utilization of LWC has emerged where lightweight aggregates were used, which resulted in reducing the structural behavior compared to columns with normal concrete. The degradation in the mechanical properties was reduced or mitigated using the combination with CFST columns where concrete was confined, and higher strength was achieved. Little research has investigated the structural behavior of LWCFST columns, including short and slender columns along with different LWC grades (normal and high strength), in depth. This study also provides a vision of the predictability of two design specifications (AISC and EC2), with comments on their safety margins and proper modification suggestions.

3. A Review of the Experimental Work

The experimental work carried out by Al-Eliwi et al. [19] was used to validate the NLFEA-simulated models, where specimens were tested under the effect of axial compressive loading. The structural behavior of CFST columns poured with lightweight concrete was examined with columns that had different length values; this resulted in different (L/D) and (D/t) ratios which were considered in the parametric study proposed in this work, along with the different concrete compressive strength values. The steel types were of mild-steel type with a circular cross-section. Specimens were divided into two groups of different cross-sections and steel yield strengths; the first one with 114.3 mm × 3.21 mm for the diameter and thickness, respectively, with a 465 MPa yielding strength compared to 114.3 mm × 5.80 mm dimensions and a 440 MPa yielding strength. The two groups had a 200 GPa modulus of elasticity. The specimens had different lengths where three

(L/D) ratios were proposed (2.62, 5.25, and 8.40), with two (D/t) values of 35.60 and 19.70 corresponding to the first and second groups, respectively.

The concrete material compressive strength of the lightweight type was obtained using 100 × 200 mm cylinders tested for their compression capacity and was found to be equal to 30.58 MPa on average. Specimens were tested using the compression testing machine, and were positioned directly at the center of the hydraulic compression jack of 3000 kN capacity to avoid any loading eccentricity. Loading was applied using the displacement control mode to ensure a uniform rate of 0.5 mm/min, which enabled the capturing of the post-peak behavior of the CFST columns where the local buckling failure was successfully captured. In addition, the amounts of shortening in the columns' ends were measured using a displacement transducer positioned within the columns' length. The values of the column end shortenings versus the compressive loading levels were measured to analyze the experimented columns' performance before and after the collapse region.

4. The Nonlinear Finite Element Analysis (NLFEA) Program

4.1. General

The NLFEA method is used in this study to examine the response of circular LWCFST columns subjected to axial loading. Before running the analysis, the CFST columns are divided into finite elements of different material or geometrical properties; each element has nodes where elements are solved using innovative algebraic formulas. Later, the theoretical formulas are formed into one global one and solved using ANSYS 16.0 [36] software to perform the simulation modeling.

4.2. Description of NLFEA

4.2.1. Element Types

The SOLID65 element was used for modeling the concrete material where the nonlinear response was efficiently simulated, in addition to the ability to capture and predict the tensile cracking, concrete crushing, and plastic deformations. The element has three freedom degrees at each one of the eight nodes forming the element. In addition, steel components (plates and tubes) were simulated using the SOLID45 element with translation capacity in all directions. Steel plates were provided at both columns' ends to avoid any stress concentration. However, two types of solid elements were used for modeling the LWC core and the outer steel tube as the SOLID65 and SOLID45 elements, where the first can capture the concrete crushing and cracking behavior while the latter one cannot. There is no need for the use of the SOLID45 element to model the steel tube behavior, since there is no cracking or crushing behavior and it is better to use an element that requires less computational time. Generally, the two solid elements can capture the compression and tension behavior of the modeled components (concrete and steel tubes).

4.2.2. Material Properties

The nonlinear compressive behavior of the stress–strain relationship in the concrete material was modeled using the multi-linear isotropic MISO relation illustrated in Figure 1, while the tensile strength was assumed to be linear with a maximum capacity equal to (f_t). Many models were examined where the results were compared between the simulated and the experimental results, including the axial vs. deflection curves along with the corresponding failure modes. However, the accurate simulation of the material characteristics and behavior requires careful examination of the general behavior and the material properties, where the experimentally reported data help in judging the resulting behavior of the different trials during the specimen's validation. The material behavior could be represented using theoretical models in the literature which prove its efficiency in predicting the structural behavior of the simulated models after well calibration and validation against experimental, analytical, or numerical data. The stress–strain behavior of lightweight concrete in compression is represented using a mathematical model established by (Almusallam and Alsayed) [37], with a 0.2 value for the Poisson's ratio. An inspection of

Figure 1 shows that the stress–strain curve starts with a linear part of the slope equal to the modulus of elasticity followed by a nonlinear part until the compressive strength is reached and the loading capacity is decreased. The open transfer shear coefficient was taken as 0.2, while the closed transfer shear coefficient was 1.0. Steel components (tubes and plates) were simulated using linear behavior with 200 GPa Young's modulus, 465 yielding stress, and 0.30 Poisson's ratio.

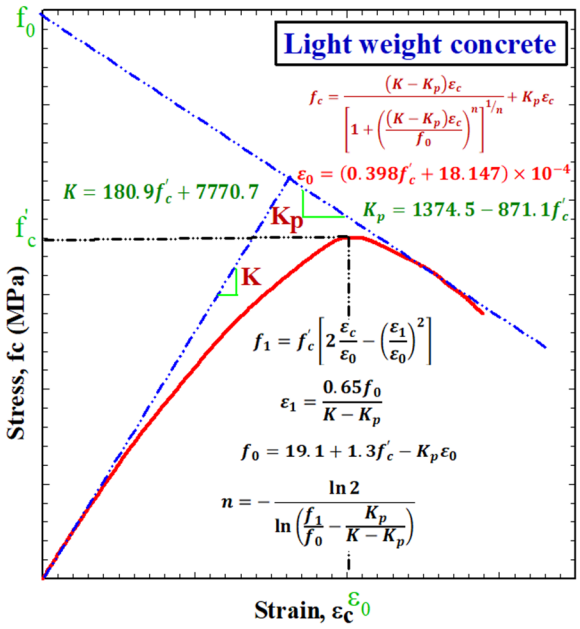

Figure 1. Concrete stress–strain curve [37].

4.2.3. Failure Criteria and Analysis

The selection criteria of the concrete material are illustrated in detail in this section, where the adopted ways for capturing the real behavior and the exact failure mode are all introduced. The failure criteria adopted in this study were proposed by William and Wranke (1975) [38], which were based on the von Mises concept. The nonlinear relationship between the stress and strain is guaranteed by defining five essential parameters, where the utilization of the William–Wranke model and the MISO plasticity models is a good choice for capturing the concrete crushing behavior and defining the failure surface. Failure occurs once the compressive or tensile stresses exceed the capacity of the loaded structural members and cause the solution to diverge. However, while the solution converges, the stress value in the perpendicular direction of the initially propagated crack is reduced to zero where stress relaxation takes place. The product of the $T_0 \times$ ft is significantly decreased, and stress is decayed, causing the solution divergence followed by a full stop in the solution process. The column has pinned boundary conditions at both ends, with the displacement being constrained in the lateral direction using the cross-sectional nodes at the bottom end. In contrast, the lateral displacements (Ux) and (Uz) were set to zero at the column's upper end. Loading was applied using small increments to ensure the solution convergence. Meshing the structural system has a direct effect on the resulting data on the ultimate capacity, ductility, and failure mode. The CFST columns were meshed in this study with a 12.5 mm size after a meshing sensitivity analysis study (Figure 2). Finally, the interaction between the outer steel tube and the inner LWC core was defined as a friction surface; however, a minimal effect was recorded since there is no actual sliding between the two interfaces.

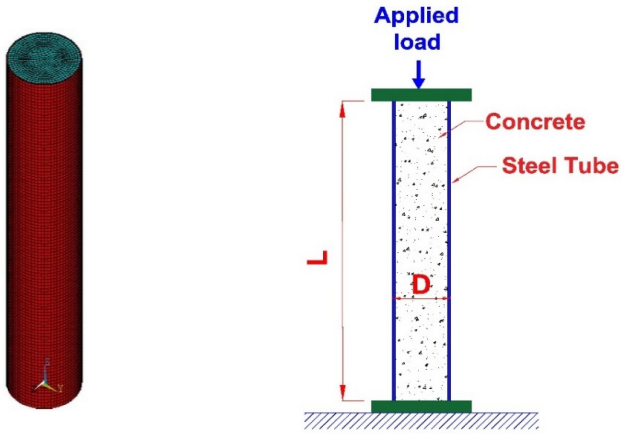

(**a**) NLFEA model (**b**) Schematic diagram

Figure 2. Typical finite element meshing and NLFEA setup.

4.3. Validation Process

After adjusting the model, six NLFEA-simulated models were validated using the experimental work conducted by Al-Eliwi et al. [19] on six specimens, as illustrated in Figure 3. The results were compared in terms of the overall compression loading versus the end shortening values. The selected specimens have three different (L/D) ratios of 2.62, 5.25, and 8.40 to represent the short, medium, and slender columns, with two (D/t) thickness values (19.70 and 35.60) to ensure the model's ability to predict the LWCFST columns under the proposed parametric study. The NLFEA and the experimental results were very close, with a 7% error percentage revealing the models' capability to capture the real structural behavior of the CFST columns.

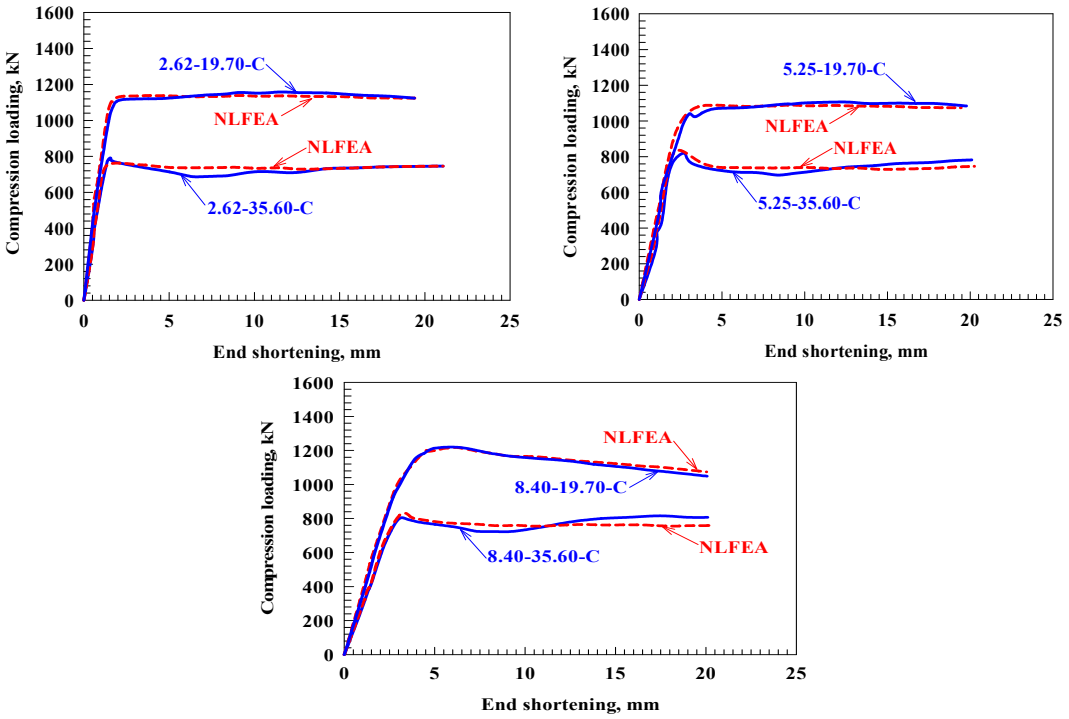

Figure 3. Compression loading versus end shortening curve for validated columns.

5. Results and Discussion

The results of the simulated-LWCFST columns are illustrated in Appendix A (Table A1), including the ultimate load, ultimate deflection, stiffness, toughness, ductility index, ca-

pacity index, and performance index. The simulated specimens were extended after the validation of the NLFEA was carried out using the experimental work of Al-Eliwi et al. [19]. The characteristics of lightweight concrete-filled steel tubular (LWCFST) columns under axial compressive load were investigated using a total of (48) LWCFST column models. The simulated models were divided into four groups with different concrete compressive strength, length-to-diameter ratios (L/D), and diameter-to-thickness ratios (D/t). Four concrete compressive values were examined (30, 40, 50, and 60 MPa), as were three length-to-diameter ratios of short (L/D = 3), medium (L/D = 6), and long (L/D = 9), and four diameter-to-thickness ratios (36, 31, 26, and 21). The specimens' designation that appears in Appendix A (Table A1) reflects the combination of the studied parameters where the first letter with the following number represents the concrete compressive strength, the second letter and its following number represents the (L/D) ratio, while the final one represents the (D/t) ratio.

5.1. Failure Modes of the LWCFST Specimens

Investigating the interaction between the steel tube, reinforcement rebars, and inner concrete core is essential to obtain the propagated composite action between the different components and their effect on the CFST columns' performance [39]. Therefore, the effects of the (L/D) and (D/t) on the concrete–steel interaction of the LWCFST columns were captured and presented in Figures 4 and 5, where the failure modes of the simulated specimens with a (D/t) ratio of 36 and an (L/D) ratio of 3 are illustrated. Generally, the local failure mode was the dominant behavior for the LWCFST columns, where specimens with higher D/t ratios experience condensed local failure regions. An inspection of Figure 4 shows that the localized buckling failure modes were clear in short specimens, with an (L/D) ratio of three.

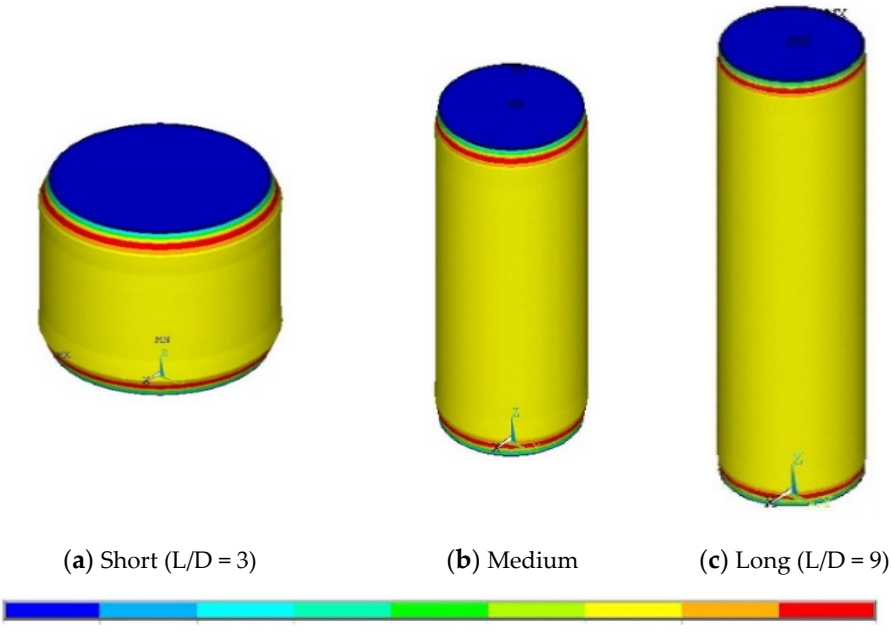

(**a**) Short (L/D = 3) (**b**) Medium (**c**) Long (L/D = 9)

Figure 4. Effect of L/D ratio on failure modes of specimens with D/t of 36.

The columns can be divided into three main categories based on their length-to-diameter value as stated by Ekmekyapar and AL-Eliwi [18], where columns with an (L/D) ratio of three are considered as short columns, while specimens with an (L/D) equal to six are medium and columns with an (L/D) ratio equal to nine are considered long. Therefore, the failure modes experienced by the LWCFST columns are highly dependent on their (L/D) ratio, where short columns experience a local buckling failure mode, the long ones (with an L/D of 9) were prone to either elastic or global buckling mode failure, while the medium column samples (with an L/D of 6) were prone to the two types of failure: the global and

local buckling modes. An inspection of Figure 4 shows that increasing the (L/D) ratio of the LWCFST columns reduces the induced stresses within the CFST columns, where increasing the (L/D) by two times reduces the maximum induced stress at failure to approximately 50%. It can be noticed that the column's length affects the compression performance of the CFST columns, as provided in the literature [18,19]. In contrast, increasing the (L/D) by three times reduces the maximum induced stress at failure to approximately 33%. The effect of the different tube thicknesses is illustrated in Figure 5 for specimens with (D/t) ratios of 21, 26, 31, and 36. Generally, increasing the tube thickness slightly affects the maximum stress value, where differences were less than 3%. On the other hand, the stress distribution is highly affected, as illustrated in Figure 5. Moreover, increasing the steel tube's thickness notably affected the local buckling at the columns' end, where the failure's size was larger when the D/t ratio was reduced (i.e., the steel tube's thickness was larger), as shown in Figure 5.

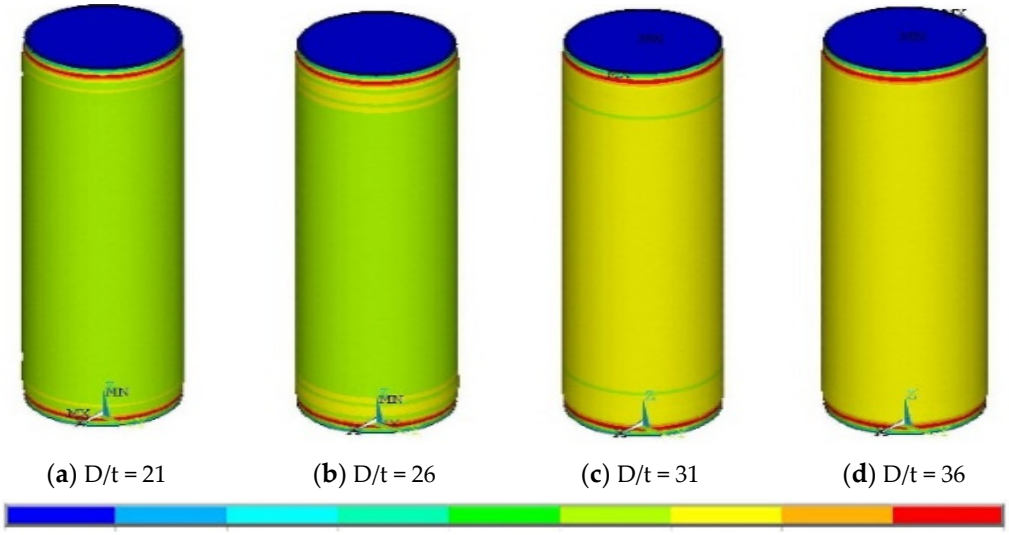

Figure 5. Effect of D/t ratio on failure modes of specimens with L/D of 9.

5.2. Compression Loading Versus End Shortening Curves

The relationship between the axial compression capacity and the end shortening is illustrated in Figure 6 for all LWCFST columns. Generally, the graph has two phases: phase 1 starts from zero and continues to the point of steel's yielding (stability point), where the loading is increased rapidly with a minor increase in the deflection values, and phase 2, where the load is minorly increased compared to rapid increasing in the deflection values. Referring to Figure 6, when the concrete's strength was increased, the compressive load increased, but the end's shortening decreased. This indicated that the column samples of high-strength concrete were more prone to brittle failure. In addition, utilizing columns with high D/t increased the compressive load and improved ductility, while columns with lower L/D increased the compressive load and ductility. The potential reason for this could be that the column with a low L/D had lower slenderness, enhancing strength and ductility more efficiently.

The behavior of the short LWCFST columns (L/D = 3) is shown in Figure 6a with different tube thicknesses, where increasing the thickness value or decreasing the (D/t) increases the compression capacity of the CFST column. In addition, the tube thickness has a direct effect on the post-peak behavior of all specimens. Thin specimens with a concrete strength of 30 MPa showed a sudden reduction in the compression loading after reaching their ultimate capacity for all columns due to the structural weakness of the lightweight aggregate combined with the contribution of the low D/t ratio which confirmed the reported conclusion by Yu et al. [40]. For thick specimens, the contribution of the concrete strength is clear; there were no sudden losses in compression capacity along

with the increase in the ultimate strength of the simulated columns. However, all specimens undergo an increase in their initial stiffness by increasing the concrete compressive strength or the steel tube thickness.

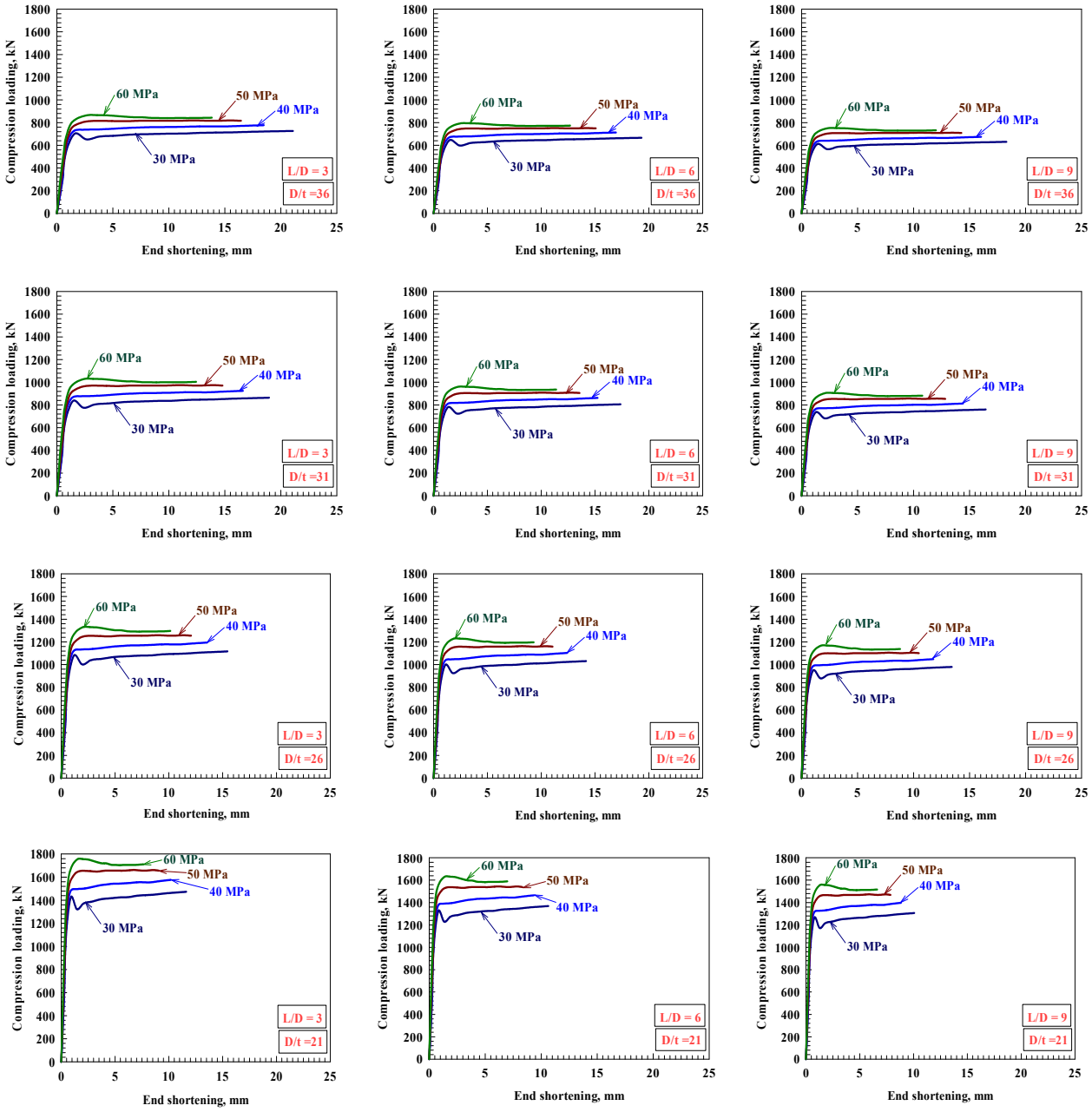

(**a**) Short (L/D = 3) (**b**) Medium (L/D = 6) (**c**) Long (L/D = 9)

Figure 6. Compression loading versus end shortening curve for NLFEA specimens.

The behavior of the medium LWCFST columns (L/D = 6) is shown in Figure 6b with different tube thicknesses, where their behavior is a combination of the behavior observed by the short and long columns. Thin specimens (D/t = 36) with a concrete strength of 30 MPa showed a sudden loss in loading after reaching compressive capacity, while no such reduction was observed for thin specimens (D/t = 36) with a concrete strength of 60 MPa. This difference in behavior shows the effect of the L/D ratio and concrete strength on the column's response. In addition, the behavior of the medium LWCFST columns (L/D = 9) is shown in Figure 6c, where their initial stiffness and ultimate compression strength are

increased by increasing the tube thickness or the concrete grade. The behavior of the thin specimens with a concrete strength of 30 MPa was similar to the short and medium columns, where local buckling failure dominated, leading to a smoother reduction in the compression load after reaching peak load. While there was no sudden reduction in loading for the thick specimens with a concrete strength of 60 MPa, and they showed a smoother transition from the pre-peak to post-peak region, the length of the column governed this behavior, which significantly differed from the behavior of short and medium columns.

5.3. Performance Indices

The performance of the LWCFST columns was examined using the stiffness, absorption of energy (or toughness), ductility index (DI) (using Equation (1)), capacity index (CI) (using Equation (2)), and performance index (PI) (using Equation (3)). Table A1 (Appendix A) displays in summary the obtained results.

$$\text{Ductility Index } (DI) = \frac{\Delta_{Ultimate}}{\Delta_{Yielding}} \quad (1)$$

The structural behavior is addressed using the ductility index (DI), where the system's ability to sustain large deformations is calculated after their elastic limit is exceeded. Table A1's (Appendix A) results show that the DI value is increased by decreasing the D/t ratio or the concrete compressive strength. In contrast, the ductility is decreased by increasing the (L/D) ratio. Figure 7a shows that increasing the concrete compressive strength to 40, 50, and 60 MPa decreases the DI capacity by 7.6, 12.7, and 13.8%, respectively. In addition, increasing the (L/D) ratio to 6 and 9 decreases the DI by 36.9% and 57.5%. Further, considering that the LWCFST columns have the same ratio of L/D, it was found that their DI was affected by the value of D/t. Also, Figure 7a revealed that using D/t values of 31, 26, and 21 enhanced DI by 34.9%, 79.2%, and 102.2%, respectively. The experiment's observations indicated that using thick steel tubes was adequate, as such tubes enhance the compression capacity of the CFST columns. However, such elements might not always ensure economic feasibility. Considering the LWCFST columns, the cores of the columns had been externally confined with a steel tube to increase the columns' compression capacity and improve the concrete's mechanical characteristics. The long and medium columns were the most influenced by this response; on the other hand, the thin columns experienced an unexpected degradation in loading due to steel tubes. The composite interaction between the concrete and steel materials affects the column's ultimate capacity, which is reflected by computing the CI (capacity index), as presented by Han et al. [41] in Equation (2). The symbols were as follows: N_u denotes the column's ultimate stress at failure; N_o denotes the column's stress at failure as per ACI 318-19 [42]; A_s denotes the steel tube's area; and A_c denotes the concrete's area.

$$CI = \frac{N_u}{N_o} = \frac{N_u}{f_y A_s + 0.85 f'_c A_c} \quad (2)$$

The computed value of the CI indicated that the column's sectional capacity was improved, as depicted in Table A1 (Appendix A). Further, Figure 7b indicated that when the concrete's strength was 40, 50, and 60 MPa, the CI was reduced by 8.1%, 15.1%, and 20.0%, respectively. In the same context, Figure 7b showed that when using D/t values of 31, 26, and 21, the CI was enhanced by 10.2%, 28.2%, and 69.2%, respectively. Also, using L/D values of 6 and 9 reduced CI by 8.3% and 13.2%, respectively. Moreover, the PI (performance index) was computed using Equation (3). An inspection of Figure 7c reveals that when the concrete's strength was 40, 50, and 60 MPa, the PI was reduced by 15.1%, 25.8%, and 31.1%, respectively. Also, when D/t was 31, 26, and 21, the PL was enhanced by 48.7%, 129.1%, and 242.1%, and increasing the L/D to 6 and 9 reduced the PI by 42.1% and 63.1%, respectively.

$$PI = DI \times CI \quad (3)$$

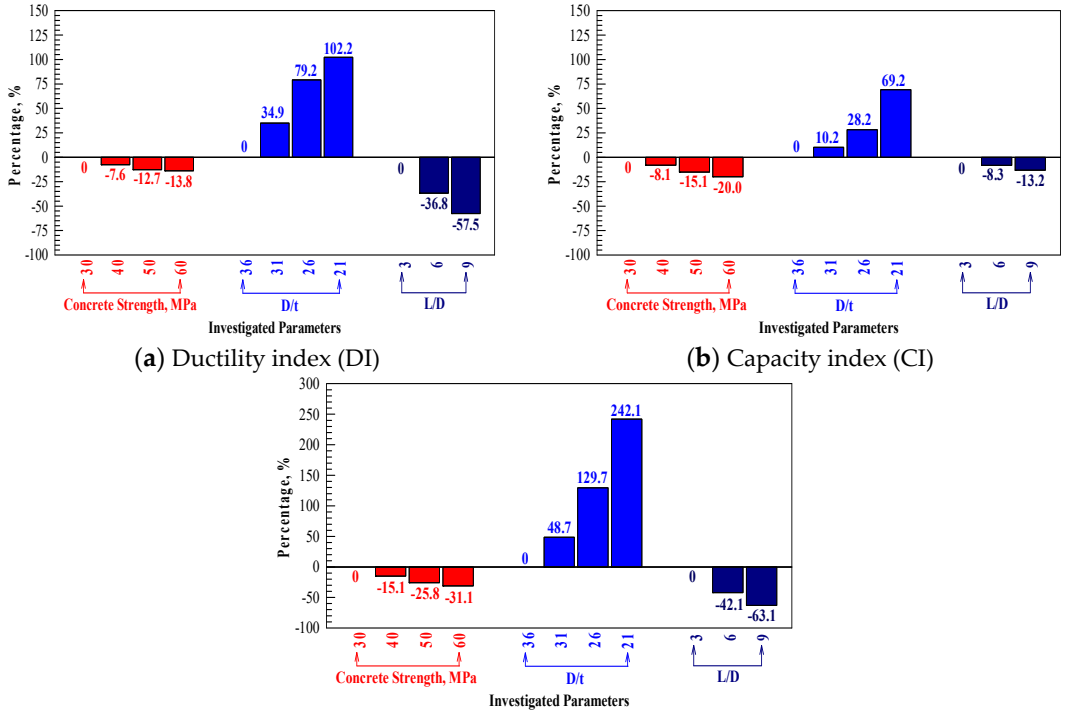

(**a**) Ductility index (DI)

(**b**) Capacity index (CI)

(**c**) Performance index (PI)

Figure 7. The DI, CI, and PI percentages versus investigated parameters.

The stiffness of the LWCFST columns is calculated as the slope of the first phase in the compression loading versus the end shortening curve. Figure 8a presents the stiffness values after being normalized with respect to the C30LD3Dt36 specimen: a column with 30 MPa lightweight concrete, a length-to-diameter ratio of 3, and a diameter-to-tube thickness of 36. An inspection of Figure 8a reveals that when the concrete's strength was 40, 50, and 60 MPa, the PI was reduced by 42.0%, 51.3%, and 64.3%, respectively. Also, when D/t was 31, 26, and 21, the PL was enhanced by 32.3%, 109.3%, and 268.3%, and increasing the L/D to 6 and 9 reduced the PI by 16.3% and 25.0%, respectively. The definition of toughness (also known as energy absorption (EA)) is the amount of energy that a substance can absorb in the plastic area until rupturing. The importance of this property lies in helping to determine structural ductility. The value of EA can be found by computing the area constrained underneath the compressive loading vs. the end's shortening graph; this area extends to a certain value of deformation (in other words, by employing either integration methods or numerical computations) [43]. The research found the value of EA by employing the numerical computations, utilizing the "trapezoidal rule formula" up to a certain level of the end's shortening. Table A1 (Appendix A) shows an enhancement in the area constrained beneath the compressive loading graph when the steel bar's area was increased. Inspecting Figure 8b reveals that when the concrete's strength was 40, 50, and 60 MPa, the EA was reduced by 5.7%, 10.3%, and 21.6%, respectively. Also, when the value of D/t was 31, 26, and 21, EA was enhanced by 7.0%, 10.3%, and 21.6%, respectively. Further, putting the value of L/D to 6 and 9 reduced EA by 15.9% and 24.7%, respectively.

The behavior of the compressive loading capacity and the column's end shortening are illustrated in Figure 9. Inspecting Figure 9a revealed that when the concrete's strength was 40, 50, and 60 MPa, the compressive loading enhanced by 7.0%, 12.8%, and 19.3%, respectively. In the same context, Figure 9a showed that when the D/t value was 31, 26, and 21, the compressive load was enhanced by 19.0%, 53.7%, and 102.8%, respectively. Also, when the value of L/D was 6 and 9, the compressive load was reduced by 8.3% and 13.2%, respectively. Further, Figure 9b revealed that when the concrete's strength was 40, 50, and 60 MPa, the end's shortening was reduced by 12.3%, 21.9%, and 34.4%, respectively. Additionally, Figure 9b indicated that when D/t was 31, 26, and 21, the end's shortening

was reduced by 10.1%, 26.7%, and 44.9%, respectively. Moreover, when the value of L/D was 6 and 9, the end's shortening decreased by 6.3% and 11.5%, respectively.

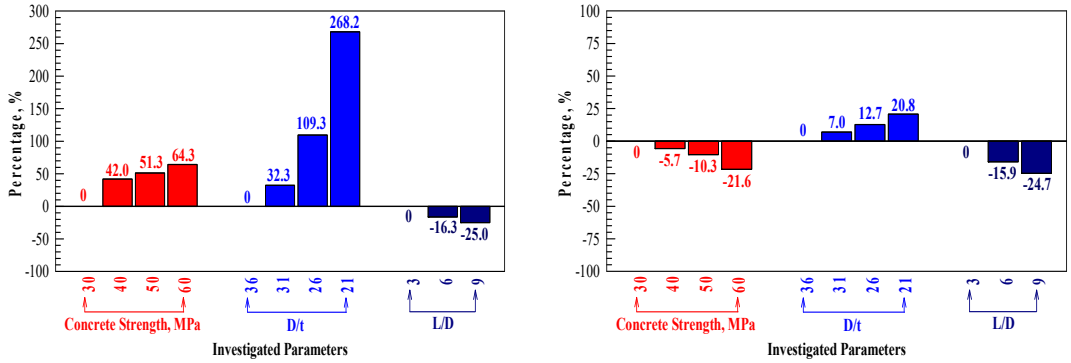

(**a**) Stiffness (k) (**b**) Energy absorption (EA)

Figure 8. The stiffness and energy absorption percentages versus investigated parameters.

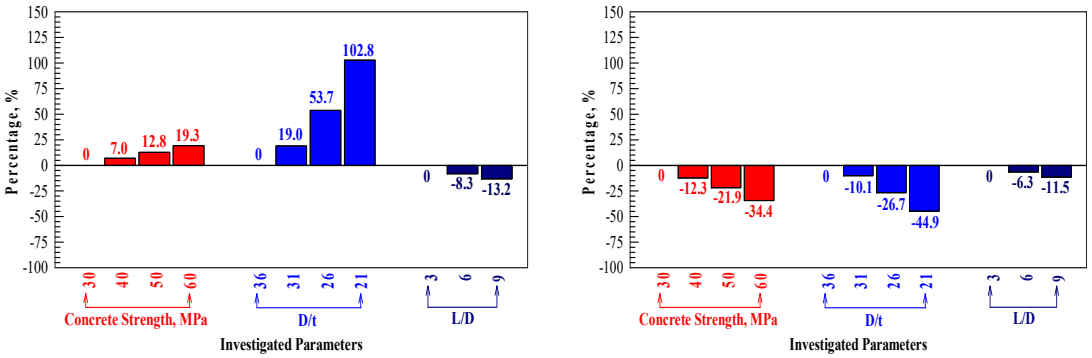

(**a**) Compression loading (P_u) (**b**) End shortening (Δ_u)

Figure 9. The compression loading and end shortening percentages versus investigated parameters.

5.4. Limitations

Despite the importance of the carried out investigation, some limitations are associated with the NLFEA results. The results apply only to CFST columns and could not be expanded for traditional columns due to the absence of the confinement effect. In addition, the results are for LWC with normal- and high-strength grades, and this does not reflect the behavior of ultra-high grades. In contrast, the results were obtained using a theoretical concrete stress–strain model which is based on the final compressive strength of the LWC mix and does not depend on the individual components of the final mixture.

6. Strength Predictions by Design Specifications

Many existing design specifications could be used to predict the CFST axial compression capacity, such as the American code ANSI/AISC360-16 [35] dealing with steel construction and the European code Eurocode4 [29], dealing with composite structures. The two codes were used in this study to predict the LWCFST-simulated columns' capacity and compared with the NLFEA results to highlight the codes' ability to predict the behavior of lightweight concrete. The EC4 [29] adopts the limit state design procedure to ensure the safety and serviceability of the designed column through the inclusion of some partial factors of safety for the applied loading and the constituent materials, as per Equation (4) to Equation (9).

$$N_{EC4} = \eta_a A_s f_y + \left(1 + \eta_c \frac{t}{D}\frac{f_y}{f_c}\right) A_c f_c \quad (4)$$

$$\eta_a = 0.25\left(3 + 2\overline{\lambda}\right) \leq 1 \quad (5)$$

$$\eta_c = 4.9 - 18.5\overline{\lambda} + 17\overline{\lambda}^2 \geq 0 \quad (6)$$

$$\overline{\lambda} = \sqrt{\frac{N_{EC4}}{N_{cr}}} \quad (7)$$

$$N_{cr} = \frac{\pi^2 E I_{eff}}{L^2} \quad (8)$$

$$EI_{eff} = E_s I_s + 0.6 E_c I_c \quad (9)$$

The A_s is the steel area, A_c is the concrete core area, f_y and f_c are the steel yielding strength and the concrete compression capacity, t is the steel tube thickness, D is the diameter of the circular cross-section, η_a and η_c are the steel and concrete amplification factors, $\overline{\lambda}$ is relative slenderness, N_{cr} is the critical compression load on the column, and E and I are the elastic modulus and moment of inertia. In the same context, the AISC360-16 code [35] permits the use of either the permissible stress design or the limit state method, as given in Equations (10) and (11) where the N_0 is the plastic strength of the column section. The outcomes of both codes were employed to find a relation between the results obtained from the codes and the ones obtained from NLFEA regarding the LWCFST columns.

$$N_{AISC} = N_0 0.658^{\frac{N_0}{N_{cr}}} \quad (10)$$

$$N_0 = P_P = A_a f_y + 0.85 A_c f_c \quad (11)$$

The outcomes obtained from AISC360-16 [35] indicated that the ratio between the actual values and the predicted ones was in a range between 0.994 and 1.157 (averaging 1.067), with a coefficient of variation (COV) of 0.041. These numbers indicated a conservative prediction, as this code's predictions were acceptable for the LWCFST columns, taking 7% as an average difference to be on the safe side. As for EC4 [29], the ratio between the actual and predicted readings was between 0.716 and 1.081 (averaging 0.880), with a COV of 0.145. The readings of EC4 [29] were not conservative by any means, with an average of 12%. Further, the average predicted value of EC4 [29] for short columns was 0.738, for medium columns was 0.857, and for long columns was 1.046. The code EC4 [29] gave un-conservative estimations for both short and medium-column samples, as they were overestimated by 26.2% for short columns and 14.3% for medium columns. Considering the long column samples, the predicted values of EC4 [29] were conservative, averaging around 4.6%. The reason behind this variation in estimations was the impact of the column's length on the confinement's performance, adding to the composite section's characteristics, mechanically and geometrically. The differences were highlighted between the code predictions and the NLFEA results in Figure 10, while the detailed numerical data are presented in Table A2 (Appendix A).

Observing Figure 10 reveals that significant differences appear between the NLFEA and the code predictions (AISC and EC4). However, it was found that the AISC360-16 [35] overestimated the axial compressive strength of CFST columns infilled with lightweight concrete, which indicates that the reduction safety factor requires an increase. In contrast, the EC4 [29] predictions approximately underestimated the axial strength with some of the cases being accurately addressed. Therefore, it could be stated that the utilization of the AISC360-16 [35] to predict the LWCFST column strength is safer in practical applications where the safety requirement is a major concern in such sensitive members.

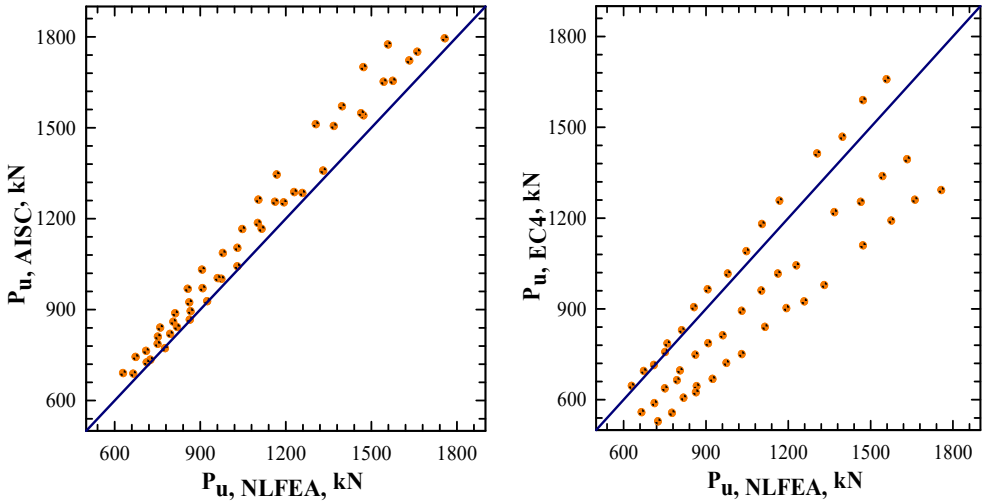

Figure 10. The NLFEA and code predictions comparison.

7. Conclusions

This study was carried out to investigate the behavior of circular LWCFST (lightweight aggregate concrete-filled circular steel tube) columns under axial compressive loads numerically using the NLFEA approach. In light of the obtained results, the following have been concluded:

1. The utilization of the CFST columns has a direct positive effect on the columns' compressive strength, toughness, and ductility where concrete is poured inside hollow steel tubes of finite thickness with the ductility being further improved by the utilization of lightweight concrete.
2. Short CFST specimens (L/D = 3) with small tube thickness (D/t = 36) have a smooth descending branch in the load–deflection curve after their maximum compression strength is reached, while specimens with larger tube thicknesses (D/t = 21) do not show any descending behavior where failure occurs suddenly.
3. Columns with medium slenderness (L/D = 6) experienced a combination failure mode between the local and global buckling, where local buckling occurs mainly for the short columns.
4. CFST columns with a length-to-diameter ratio exceeding nine and a small steel tube thickness behave similarly to the medium slenderness column where the failure was a combination of the local and global buckling. In contrast, larger tube thicknesses (D/t = 21) experienced global buckling failure.
5. Providing steel tubes to the conventionally utilized RC columns increases their compression capacity, with the behavior being preferable for thin steel tubes of both long and short columns. In addition, increasing the compressive strength of the used lightweight concrete further improves their structural behavior. In contrast, CFST columns with a medium length-to-diameter ratio had their maximum capacity with thick steel tubes.
6. The predicted compressive strength capacities of the LWCFST columns given by AISC360-16 were conservative, with a difference percentage reaching 4% from the values provided by the NLFEA. On the other hand, the estimations of EC4 were not conservative, with a 12% difference percentage.

Author Contributions: Conceptualization, R.A.-R. and B.R.A.; methodology, R.A.-R. and B.R.A.; formal analysis, R.A.-R. and B.R.A.; investigation, R.A.-R. and B.R.A.; resources, R.A.-R. and B.R.A.; data curation, R.A.-R. and B.R.A.; writing—original draft preparation, R.A.-R. and B.R.A.; writing—review and editing, B.R.A.; visualization, R.A.-R. and B.R.A.; supervision, R.A.-R. and B.R.A.; project administration, R.A.-R. and B.R.A. All authors have read and agreed to the published version of the manuscript.

Funding: This research received no external funding.

Data Availability Statement: Data will be made available on request.

Acknowledgments: This work was fully supported by Jordan University of Science and this support is gratefully acknowledged.

Conflicts of Interest: The authors declare no conflicts of interest.

Appendix A

Table A1. NLFEA column's designation and results.

Column	f_c', MPa	L/D	D/t	Δu, mm	Pu, kN	K, kN/mm	EA, kN·mm	DI	CI	PI
C30LD3Dt36	30	3	36	21.08	726	257	14,385	2.534	0.911	2.309
C40LD3Dt36	40			18.48	777	365	13,568	2.340	0.837	1.960
C50LD3Dt36	50			16.45	819	389	12,908	2.213	0.774	1.712
C60LD3Dt36	60			13.83	867	423	11,275	2.183	0.729	1.591
C30LD3Dt31	30		31	18.95	864	340	15,387	3.419	1.004	3.434
C40LD3Dt31	40			16.62	925	483	14,513	3.209	0.933	2.993
C50LD3Dt31	50			14.79	975	515	13,807	3.008	0.868	2.612
C60LD3Dt31	60			12.43	1031	559	12,060	2.909	0.823	2.394
C30LD3Dt26	30		26	15.45	1116	539	16,207	4.540	1.168	5.302
C40LD3Dt26	40			13.55	1194	765	15,287	4.278	1.099	4.702
C50LD3Dt26	50			12.06	1259	815	14,542	3.806	1.034	3.936
C60LD3Dt26	60			10.14	1332	886	12,703	3.740	0.988	3.695
C30LD3Dt21	30		21	11.61	1473	947	16,551	5.123	1.541	7.896
C40LD3Dt21	40			10.18	1576	1345	15,611	4.827	1.451	7.003
C50LD3Dt21	50			9.06	1662	1432	14,850	4.433	1.365	6.049
C60LD3Dt21	60			7.62	1758	1556	12,972	4.221	1.304	5.504
C30LD6Dt36	30	6	36	19.33	666	215	12,096	1.601	0.836	1.338
C40LD6Dt36	40			16.95	713	306	11,408	1.479	0.768	1.135
C50LD6Dt36	50			15.08	751	326	10,853	1.390	0.709	0.986
C60LD6Dt36	60			12.68	795	354	9480	1.344	0.668	0.898
C30LD6Dt31	30		31	17.38	806	293	13,156	2.237	0.936	2.095
C40LD6Dt31	40			15.24	862	416	12,408	2.108	0.870	1.833
C50LD6Dt31	50			13.56	909	443	11,804	1.923	0.810	1.557
C60LD6Dt31	60			11.40	962	482	10,311	1.843	0.767	1.415
C30LD6Dt26	30		26	14.17	1031	465	13,724	2.854	1.078	3.078
C40LD6Dt26	40			12.43	1103	661	12,944	2.690	1.015	2.730
C50LD6Dt26	50			11.06	1163	704	12,314	2.470	0.955	2.358
C60LD6Dt26	60			9.30	1230	765	10,756	2.352	0.912	2.146
C30LD6Dt21	30		21	10.64	1369	842	14,101	3.298	1.432	4.723
C40LD6Dt21	40			9.34	1465	1196	13,300	2.972	1.348	4.005
C50LD6Dt21	50			8.31	1544	1274	12,652	2.753	1.268	3.490
C60LD6Dt21	60			6.98	1634	1383	11,052	2.662	1.211	3.225

Table A1. *Cont.*

Column	f'_c, MPa	L/D	D/t	Δu, mm	Pu, kN	K, kN/mm	EA, kN·mm	DI	CI	PI
C30LD9Dt36	30	9	36	18.29	630	193	10,831	1.178	0.791	0.852
C40LD9Dt36	40			16.04	674	274	10,216	1.116	0.727	0.738
C50LD9Dt36	50			14.27	711	292	9718	1.090	0.671	0.607
C60LD9Dt36	60			12.00	752	317	8489	1.088	0.632	0.561
C30LD9Dt31	30		31	16.44	760	265	11,739	1.465	0.883	1.294
C40LD9Dt31	40			14.42	813	377	11,073	1.353	0.820	1.110
C50LD9Dt31	50			12.84	857	402	10,533	1.280	0.764	0.977
C60LD9Dt31	60			10.79	907	436	9201	1.263	0.724	0.914
C30LD9Dt26	30		26	13.41	980	431	12,344	1.854	1.025	1.901
C40LD9Dt26	40			11.76	1048	612	11,643	1.740	0.965	1.679
C50LD9Dt26	50			10.47	1105	652	11,076	1.633	0.908	1.482
C60LD9Dt26	60			8.80	1169	708	9675	1.611	0.867	1.397
C30LD9Dt21	30		21	10.07	1306	784	12,733	2.159	1.367	2.951
C40LD9Dt21	40			8.83	1398	1113	12,010	1.964	1.286	2.526
C50LD9Dt21	50			7.86	1473	1186	11,425	1.841	1.210	2.227
C60LD9Dt21	60			6.61	1559	1288	9980	1.780	1.156	2.058

Note: f'_c is the concrete compressive strength; Δu is the ultimate end shortening; Pu is the ultimate compression loading; K is the stiffness; EA is the energy absorption; DI is the ductility index (Equation (1)); CI is the capacity index (Equation (2)); and PI is the performance index (Equation (3)).

Table A2. The NLFEA results versus ANSI/AISC360-16 [35] and Eurocode4 [29].

Column	$P_{u,NLFEA}$, kN	$P_{u,AISC}$, kN	$\frac{P_{u,AISC}}{P_{u,NLFEA}}$	$P_{u,EC4}$, kN	$\frac{P_{u,EC4}}{P_{u,NLFEA}}$
C30LD3Dt36	726	734	1.010	528	0.727
C40LD3Dt36	777	772	0.994	556	0.716
C50LD3Dt36	819	842	1.027	606	0.740
C60LD3Dt36	867	894	1.031	644	0.742
C30LD3Dt31	864	866	1.003	624	0.722
C40LD3Dt31	925	927	1.003	668	0.722
C50LD3Dt31	975	1001	1.027	721	0.740
C60LD3Dt31	1031	1042	1.011	750	0.728
C30LD3Dt26	1116	1166	1.045	840	0.752
C40LD3Dt26	1194	1253	1.049	902	0.755
C50LD3Dt26	1259	1284	1.020	924	0.734
C60LD3Dt26	1332	1358	1.020	978	0.734
C30LD3Dt21	1473	1540	1.045	1109	0.753
C40LD3Dt21	1576	1654	1.049	1191	0.756
C50LD3Dt21	1662	1750	1.053	1260	0.758
C60LD3Dt21	1758	1794	1.020	1292	0.735
C30LD6Dt36	666	688	1.034	558	0.837
C40LD6Dt36	713	725	1.018	588	0.824

Table A2. *Cont.*

Column	$P_{u,NLFEA}$, kN	$P_{u,AISC}$, kN	$\frac{P_{u,AISC}}{P_{u,NLFEA}}$	$P_{u,EC4}$, kN	$\frac{P_{u,EC4}}{P_{u,NLFEA}}$
C50LD6Dt36	751	786	1.046	637	0.848
C60LD6Dt36	795	819	1.030	664	0.835
C30LD6Dt31	806	859	1.066	696	0.863
C40LD6Dt31	862	923	1.071	748	0.867
C50LD6Dt31	909	970	1.068	786	0.865
C60LD6Dt31	962	1003	1.043	812	0.845
C30LD6Dt26	1031	1103	1.070	893	0.867
C40LD6Dt26	1103	1185	1.075	960	0.871
C50LD6Dt26	1163	1255	1.079	1016	0.874
C60LD6Dt26	1230	1287	1.046	1043	0.848
C30LD6Dt21	1369	1505	1.099	1219	0.890
C40LD6Dt21	1465	1547	1.056	1253	0.855
C50LD6Dt21	1544	1651	1.070	1338	0.866
C60LD6Dt21	1634	1721	1.053	1394	0.853
C30LD9Dt36	630	690	1.094	645	1.023
C40LD9Dt36	674	743	1.101	694	1.030
C50LD9Dt36	711	763	1.074	714	1.004
C60LD9Dt36	752	810	1.076	757	1.006
C30LD9Dt31	760	840	1.106	785	1.034
C40LD9Dt31	813	887	1.091	829	1.020
C50LD9Dt31	857	968	1.130	905	1.057
C60LD9Dt31	907	1031	1.137	964	1.063
C30LD9Dt26	980	1086	1.109	1016	1.037
C40LD9Dt26	1048	1165	1.111	1090	1.039
C50LD9Dt26	1105	1262	1.142	1180	1.068
C60LD9Dt26	1169	1345	1.150	1257	1.075
C30LD9Dt21	1306	1511	1.157	1413	1.081
C40LD9Dt21	1398	1570	1.123	1468	1.050
C50LD9Dt21	1473	1699	1.153	1589	1.078
C60LD9Dt21	1559	1774	1.138	1658	1.064

Note: $P_{u,NLFEA}$ is the NLFEA ultimate compression loading capacity; $P_{u,AISC}$ is the ultimate compression loading capacity according to ANSI/AISC360-16; $P_{u,EC4}$ is the ultimate compression loading capacity according to Eurocode4.

References

1. Han, L.-H.; Li, W.; Bjorhovde, R. Developments and advanced applications of concrete-filled steel tubular (CFST) structures: Members. *J. Constr. Steel Res.* **2014**, *100*, 211–228. [CrossRef]
2. Al-Rousan, R.Z.; Alnemrawi, B.R.; Sawalha, H.M. The ultimate capacity of geopolymer recycled aggregate concrete filled steel tubular columns: Numerical and theoretical study. *J. Build. Eng.* **2024**, *96*, 110365. [CrossRef]
3. Liew, J.Y.R.; Xiong, M.; Xiong, D. Design of Concrete Filled Tubular Beam-columns with High Strength Steel and Concrete. *Structures* **2016**, *8*, 213–226. [CrossRef]
4. Romero, M.L.; Ibañez, C.; Espinos, A.; Portolés, J.M.; Hospitaler, A. Influence of Ultra-high Strength Concrete on Circular Concrete-filled Dual Steel Columns. *Structures* **2017**, *9*, 13–20. [CrossRef]
5. Hassanein, M.F.; Elchalakani, M.; Karrech, A.; Patel, V.I.; Yang, B. Behaviour of Concrete-filled Double-skin Short Columns Under Compression Through Finite Element Modelling: SHS Outer and SHS Inner Tubes. *Structures* **2018**, *14*, 358–375. [CrossRef]

6. Ekmekyapar, T. Experimental performance of concrete filled welded steel tube columns. *J. Constr. Steel Res.* **2016**, *117*, 175–184. [CrossRef]
7. Abdalla, K.M.; Al-Rousan, R.; Alhassan, M.A.; Lagaros, N.D. Finite-element modelling of concrete-filled steel tube columns wrapped with CFRP. *Proc. Inst. Civ. Eng.-Struct. Build.* **2020**, *173*, 844–857. [CrossRef]
8. Al-Rousan, R.Z.; Alnemrawi, B.R. Cyclic Behavior of CFRP Confined Circular CFST Damaged by Alkali-Silica Reaction. *Int. J. Civ. Eng.* **2023**, *21*, 1159–1180. [CrossRef]
9. Chan, T.-M.; Huai, Y.-M.; Wang, W. Experimental investigation on lightweight concrete-filled cold-formed elliptical hollow section stub columns. *J. Constr. Steel Res.* **2015**, *115*, 434–444. [CrossRef]
10. Serras, D.N.; Skalomenos, K.A.; Hatzigeorgiou, G.D.; Beskos, D.E. Modeling of circular concrete-filled steel tubes subjected to cyclic lateral loading. *Structures* **2016**, *8*, 75–93. [CrossRef]
11. Wang, J.; Wang, J.; Wang, H. Seismic Behavior of Blind Bolted CFST Frames with Semi-rigid Connections. *Structures* **2017**, *9*, 91–104. [CrossRef]
12. *ASTMC330/C330M−17*; Standard Specification for Lightweight Aggregates for Structural Concrete. ASTM International: West Conshohocken, PA, USA, 2017.
13. *ACI213R-03*; Guide for Structural Lightweight-Aggregate Concrete. American Concrete Institute: Farmington Hills, MI, USA, 2003.
14. Zhou, Y.; Liu, X.; Xing, F.; Cui, H.; Sui, L. Axial compressive behavior of FRP-confined lightweight aggregate concrete: An experimental study and stress-strain relation model. *Constr. Build. Mater.* **2016**, *119*, 1–15. [CrossRef]
15. Fu, Z.; Ji, B.; Lv, L.; Yang, M. The mechanical properties of lightweight aggregate concrete confined by steel tube. *Des. Constr. Rehabil. Maint. Bridges* **2011**, 33–39.
16. Kanagaraj, B.; Anand, N.; Praveen, B.; Kandasami, S.; Lubloy, E.; Naser, M.Z. Physical characteristics and mechanical properties of a sustainable lightweight geopolymer based self-compacting concrete with expanded clay aggregates. *Dev. Built Environ.* **2023**, *13*, 100115. [CrossRef]
17. de Oliveira, W.L.A.; De Nardin, S.; de Cresce El Debs, A.L.H.; El Debs, M.K. Influence of concrete strength and length/diameter on the axial capacity of CFT columns. *J. Constr. Steel Res.* **2009**, *65*, 2103–2110. [CrossRef]
18. Ekmekyapar, T.; Al-Eliwi, B.J.M. Experimental behaviour of circular concrete filled steel tube columns and design specifications. *Thin-Walled Struct.* **2016**, *105*, 220–230. [CrossRef]
19. Al-Eliwi, B.J.M.; Ekmekyapar, T.; Al-Samaraie, M.I.A.; Doğru, M.H. Behavior of Reinforced Lightweight Aggregate Concrete-filled Circular Steel Tube Columns Under Axial Loading. *Structures* **2018**, *16*, 101–111. [CrossRef]
20. Al-Rousan, R.; Nusier, O.; Abdalla, K.; Alhassan, M.; Lagaros, N.D. NLFEA of Sulfate-Damaged Circular CFT Steel Columns Confined with CFRP Composites and Subjected to Axial and Cyclic Lateral Loads. *Buildings* **2022**, *12*, 296. [CrossRef]
21. Al-Rousan, R.Z.; Sawalha, H.M. The behavior of concrete filled steel tubular columns infilled with high-strength geopolymer recycled aggregate concrete. *Steel Compos. Struct.* **2024**, *51*, 661. [CrossRef]
22. Zhong-qiu, F.; Bo-hai, J.; Lei, L.; Wen-jie, Z.J.I.-X. Behavior of lightweight aggregate concrete filled steel tubular slender columns under axial compression. *Adv. Steel Constr.* **2011**, *7*, 144–156. [CrossRef]
23. Zhou, Y.; Liu, X.; Xing, F.; Li, D.; Wang, Y.; Sui, L. Behavior and modeling of FRP-concrete-steel double-skin tubular columns made of full lightweight aggregate concrete. *Constr. Build. Mater.* **2017**, *139*, 52–63. [CrossRef]
24. Al-Rousan, R.Z.; Barfed, M.H. Impact of curvature type on the behavior of slender reinforced concrete rectangular column confined with CFRP composite. *Compos. Part B Eng.* **2019**, *173*, 106939. [CrossRef]
25. Xue, H.; Zhao, K.; Xia, F.; Wang, G.; Shen, A. Numerical Investigation of the Ultimate Load-Carrying Capacity of Square Concrete-Filled Steel Tube Columns Considering Initial Stresses Generated during Construction. *Buildings* **2023**, *13*, 2830. [CrossRef]
26. Ghannam, S.; Jawad, Y.A.; Hunaiti, Y. Failure of lightweight aggregate concrete-filled steel tubular columns. *Steel Compos. Struct.* **2004**, *4*, 1–8. [CrossRef]
27. Mouli, M.; Khelafi, H. Strength of short composite rectangular hollow section columns filled with lightweight aggregate concrete. *Eng. Struct.* **2007**, *29*, 1791–1797. [CrossRef]
28. Fu, Z.; Ji, B.; Zhou, Y.; Wang, X. An experimental behavior of lightweight aggregate concrete filled steel tubular stub under axial compression. *Des. Constr. Rehabil. Maint. Bridges* **2011**, 24–32.
29. EC4. *Design of Composite Steel and Concrete Structures-Part 1-1: General Rules and Rules for Buildings*; European Committee for Standardization: Brussels, Belgium, 2004.
30. Ji, B.; Fu, Z.; Qu, T.; Wang, M. Stability behavior of lightweight aggregate concrete filled steel tubular columns under axial compression. *Adv. Steel Constr.* **2013**, *9*, 1–13. [CrossRef]
31. AL-Eliwi, B.J.; Ekmekyapar, T.; Faraj, R.H.; Göğüş, M.T.; AL-Shaar, A.A. Performance of lightweight aggregate and self-compacted concrete-filled steel tube columns. *Steel Compos. Struct.* **2017**, *25*, 299–314. [CrossRef]
32. Al-Rousan, R.; Alnemrawi, B.R. NLFEA of the Behavior of Polypropylene-Fiber-Reinforced Concrete Slabs with Square Opening. *Buildings* **2024**, *14*, 480. [CrossRef]
33. Memarzadeh, A.; Shahmansouri, A.A.; Pologanathan, K. A novel prediction model for post-fire elastic modulus of circular recycled aggregate concrete-filled steel tubular stub columns. *Steel Compos. Struct. Int. J.* **2022**, *44*, 309–324. [CrossRef]

34. Akbarzadeh Bengar, H.; Shahmansouri, A.A. Post-fire behavior of unconfined and steel tube confined rubberized concrete under axial compression. *Structures* **2021**, *32*, 731–745. [CrossRef]
35. *ANSI/AISC360-16*; Specification for Structural Steel Buildings. American Institute of Steel Construction: Chicago, IL, USA, 2016.
36. ANSYS. *ANSYS User's Manual Revision 16.0*; ANSYS, Inc.: Canonsburg, PA, USA, 2016.
37. Almusallam, T.H.; Alsayed, S.H. Stress–strain relationship of normal, high-strength and lightweight concrete. *Mag. Concr. Res.* **1995**, *47*, 39–44. [CrossRef]
38. Willam, K.; Warnke, E. Constitutive model for the triaxial behavior of concrete. *Int. Assoc. Bridge Struct. Eng.* **1975**, *19*, 1–30. [CrossRef]
39. Roeder, C.W.; Cameron, B.; Brown, C.B. Composite Action in Concrete Filled Tubes. *J. Struct. Eng.* **1999**, *125*, 477–484. [CrossRef]
40. Yu, X.; Tao, Z.; Song, T.-Y. Effect of different types of aggregates on the performance of concrete-filled steel tubular stub columns. *Mater. Struct.* **2016**, *49*, 3591–3605. [CrossRef]
41. Han, L.-H.; Yao, G.-H.; Zhao, X.-L. Tests and calculations for hollow structural steel (HSS) stub columns filled with self-consolidating concrete (SCC). *J. Constr. Steel Res.* **2005**, *61*, 1241–1269. [CrossRef]
42. ACI 318. *Building Code Requirements for Reinforced Concrete and Commentary*; American Concrete Institute: Farmington Hills, MI, USA, 2019.
43. Ezeldin, A.S.; Balaguru, P.N. Normal- and High-Strength Fiber-Reinforced Concrete under Compression. *J. Mater. Civ. Eng.* **1992**, *4*, 415–429. [CrossRef]

Disclaimer/Publisher's Note: The statements, opinions and data contained in all publications are solely those of the individual author(s) and contributor(s) and not of MDPI and/or the editor(s). MDPI and/or the editor(s) disclaim responsibility for any injury to people or property resulting from any ideas, methods, instructions or products referred to in the content.